Laser-induced plasma spectroscopy of hydrogen-nitrogen mixtures

CHRSTIAN G. PARIGGER

Physics and Astronomy Department, University of Tennessee, University of Tennessee Space Institute,
Center for Laser Applications, 411 B.H. Goethert Parkway, Tullahoma, TN 37388-9700, USA
E-mail: cparigge@tennessee.edu

ABSTRACT: This work reports recent laser-plasma experiments that measure electron density and temperature from the first four members of the Balmer series, namely, Hα, Hβ, Hγ, and Hδ lines. The laboratory micro-plasma expands in a 1:1, 0.27-atm gaseous mixture of hydrogen and nitrogen following generation with Nd:YAG, Q-switched, 150-mJ and 6-ns pulses. Time-resolved emission spectroscopy examines the spatial and temporal aspects of the expansion dynamics. For 13 equally spaced time delays from 0.25 μs to 3.25 μs and 0.025-μs gate-widths, micro-plasma diagnostics is evaluated. Of interest are spatially-resolved evaluations of the peak-separation and width of Hδ and width of Hγ for electron densities in the range of 0.1 to 1×10^{17} cm^{-3}, spatially-resolved temperature determination from Boltzmann plots, and comparisons with Hα and Hβ diagnostics. Integral inversions interrogate spatial distributions of the plasma expansion. Applications include laboratory and stellar astrophysics plasma characterizations.

PACS Codes: 52.70.-m, 32.30-r, 52.25.Jm, 42.62.Fi

Keywords: Plasma diagnostics, atomic spectra, plasma spectroscopy, laser spectroscopy, laser-induced breakdown spectroscopy.

1. INTRODUCTION

Laser-induced optical breakdown in gases such as laboratory air generates a laser-plasma that propagates initially at well-above hypersonic speed. Subsequently, the shock-wave expansion speed is supersonic for time delays of the order of 1μs, approaching sonic speed for time delays of the order of 10 to 100 μs. Focusing Nd:YAG Q-switched pulses to irradiances slightly above optical breakdown threshold in air produces a spherically symmetric shockwave that can be measured using fast photography techniques. However, plasma spectroscopy delivers detailed species distribution over and above electron density and local temperature and finds a variety of applications of laser-induced breakdown spectroscopy [1,2]. Accurate understanding of laser-plasma is desirable for analytic evaluations of the plasma composition [3,4]. Addition of hydrogen is suggested [5] for plasma spectroscopy [6,7] that comprises spatially- and temporally- resolved investigations that usually extend to applications of integral inversions [8] of measured line-of-sight data.

The aim of the experiments includes establishment of a reliable diagnosis of the early, fluid-dynamics dominated expansion associated with optical breakdown. To accomplish this task, a 1:1 mixture of hydrogen and nitrogen gases at a pressure of 0.27 atm is selected. Spatially- and temporally resolved spectroscopy of the first four Balmer series members delivers local plasma parameters, namely, electron density, N_e, and temperature, T_e, from recorded Hα, Hβ, Hγ, and Hδ line shapes. The emitted plasma radiation is imaged onto the slit of a Czerny-Turner type spectrometer fitted with a two-dimensional intensified charge-coupled device (ICCD) to yield spatial resolution along the slit-dimension. The line-of-sight data are also analyzed using integral inversion techniques.

This work also establishes comparisons of laser-spectroscopy inferences with shadow-graphs recorded in laboratory air utilizing irradiance levels well-above optical breakdown threshold. Noteworthy, the speed of sound in hydrogen exceeds that in air by a factor of 3.8. Consequently, recorded shadow-graphs in air at a time delay of, say, 1 μs approximately correspond to a time delay of 3.8 μs in hydrogen.

Moreover, goals of the reported experimental investigations include evaluation of electron density diagnostics using Hδ line shapes with standard double-peak profiles due to Stark effect predictions, viz. a splitting just like Hβ. The Hγ line shape is also investigated experimentally and compared with predicted line shapes using standard Stark tables [9]. Of course, objectives are evaluation of laser-plasma electron density from the full-width half-maximum (FWHM) of all four lines – for electron densities in the range 0.1 to 1×10^{17} cm^{-3}. For electron density in the range of 1 to 4×10^{17} cm^{-3}, measurement of Hβ FWHM is recommended, and in the range of 4 to 20×10^{17} cm^{-3}, FWHM of Hα works well, but above 50×10^{17} cm^{-3} self-absorption effects for Hα FWHM measurements are considerable. However, peak-separation of Hβ and shifts of Hα can provide reasonable values for electron density.

Applications of the reported experimental work include analysis of stellar astrophysical spectra from white dwarf stars [10]. In the visible region of the electromagnetic spectrum, Hβ is of primary interest in the characterization of white dwarf (WD) stars. However, comparisons of a set of hydrogen Balmer-series emission lines with recorded astrophysical WD absorption lines requires bound-free opacity corrections [10]. Challenges in comparisons of laboratory and astrophysical plasma-spectra have been reviewed recently [11], i.e., comparisons of Hβ line shapes of micro-plasma recorded with time-resolved emission spectroscopy and of Hβ line shapes in astrophysical white dwarf macro-plasma absorption spectra that are measured continuously at various observatories.

2. EXPERIMENTAL DETAILS

Laboratory laser-plasma measurements employ a pulsed, Q-switched, Nd:YAG laser device (Q-Smart 850 Quantel laser) operated at a pulse-width of 6 ns and a pulse energy of 850 mJ at the wavelength of 1064 nm. Laser-induced optical breakdown is generated by focusing 150 mJ per pulse of ir fundamental radiation to achieve an irradiance of the order of 1 TW/cm^2 in a cell containing a 1:1 mixture of hydrogen and nitrogen, introduced at a pressure of 0.135 atm each after establishing a nominal mercury-diffusion-pump vacuum in the cell of the order 10^{-5} mbar. A crossed Czerny – Turner spectrometer (Jobin Yvon 0.64 m triple spectrometer) of 0.64-nm focal length disperses the emission spectra. The pulsed radiation is focused into the cell with the beam propagating from the top and parallel to the vertical 100 μm spectrometer slit. Further details of the experimental arrangement, analogous to the ultra-pure hydrogen experiments, were communicated previously [12,13].

The spectral resolution amounts to 0.1 nm for the selected 1200 g mm^{-1} holographic grating following corrections of the wavelength variation along the slit direction [14]. Of the order of 24-nm spectral coverage for the 1024 pixels along the wavelength-dimension, the 0.1-nm resolution corresponds to an instrument-prompt width of on-average 4.25 pixels. Grouping four pixels along the slit dimensions corresponds to a spatial resolution of 54.4 μm as the pixel area amounts to 13.6 μm × 13.6 μm.

3. RESULTS AND DISCUSSION

For 13 selected time delays from 0.25 μs to 3.25 μs and 0.025 μs gate-widths, micro-plasma data are captured. Of interest are Balmer series Stark-effects [15-19] including the peak-separation and width of Hδ and width of Hγ for electron densities in the range of 0.1 to 1×10^{17} cm^{-3}, and comparisons with Hβ and Hα diagnostics. Integral inversions interrogate the spatial distributions of the recorded line-of-sight plasma expansion.

3.1 Line-of-sight measurements

A total of 52 two-dimensional data sets are recorded for the four Hα, Hβ, Hγ, and Hδ Balmer series lines, including several nitrogen and ionized nitrogen lines especially for time delays in the range of 0.25 - 0.75 μs following plasma

initiation. Figures 1 to 4 illustrate spectral radiance, pseudo-colored, individually scaled maps of the four hydrogen lines for time delays of 0.75, 1.5, 2.25, and 3.25 μs.

Features of Figure 1 include, (i) full-widths at half maximum increase from the Hα line to the Hγ line; (ii) the maximum decreases from Hα to Hγ; (iii) occurrence of a neutral nitrogen line near 399 nm in the Hδ map above a uv-shaded background – the broad Hδ line will show a peak separation for larger time delays; (iv) peak-separation of the Hβ line, or the occurrence of a dip – this dip is not due to self-absorption – prediction of the Stark effect for the Hβ line is part of the reason for E. Schrödinger's [19] Nobel Prize in Physics in 1933 [20], shared with P. Dirac.

In the images, detector dark-counts or background contributions are subtracted, sensitivity calibrations by reference to standard lamps are applied, and linear wavelength calibration is performed with penray lamps and by using calibrated spectrometer dials. The image of the spectrometer slit usually is slightly curved near the edges, consequently, wavelength calibrations are performed for each spectrum recorded along the slit. For the experiments reported here, four vertical pixels are combined to increase sensitivity requiring 256 individual wavelength calibrations for each of four spectrometer positions. The 256 recorded, wavelength calibrated Balmer series spectra are slightly shifted and interpolated for display of the data versus slit height and wavelength position. In other words, the displayed maps are corrected for wavelength variations along the slit dimension.

Analysis of the laboratory emission spectra utilizes established empirical formulae for Hα and Hβ [12]. For Hα, the width, $\Delta\lambda_\alpha$, and shift, $\delta\lambda_\alpha$, are indicators for electron density,

$$\Delta\lambda_\alpha[\text{nm}] = 1.3 \left(\frac{N_e[\text{cm}^{-3}]}{10^{17}}\right)^{0.64 \pm 0.03} \tag{1}$$

$$\delta\lambda_\alpha[\text{nm}] = 0.055 \left(\frac{N_e[\text{cm}^{-3}]}{10^{17}}\right)^{0.97 \pm 0.03} \tag{2}$$

Analysis of Hβ offers three indicators for electron density determination: Width, $\Delta\lambda_\beta$, peak separation, $\Delta\lambda_{\beta-ps}$, and dip shift, $\delta\lambda_{\beta-ds}$,

$$\Delta\lambda_\beta[\text{nm}] = 4.5 \left(\frac{N_e[\text{cm}^{-3}]}{10^{17}}\right)^{0.71 \pm 0.03} \tag{3}$$

$$\delta\lambda_{\beta-ps}[\text{nm}] = 1.3 \left(\frac{N_e[\text{cm}^{-3}]}{10^{17}}\right)^{0.61 \pm 0.03} \tag{4}$$

$$\delta\lambda_{\beta-ds}[\text{nm}] = 0.14 \left(\frac{N_e[\text{cm}^{-3}]}{10^{17}}\right)^{0.67 \pm 0.03}. \tag{5}$$

The Hβ dip-shift allows one to measure electron density [11] up to the Hβ Inglis-Teller limit [21] of 60×10^{17} cm^{-3}.

However, Hβ is preferred for astrophysics data-reduction efforts for electron densities of the order of 10^{17} cm^{-3}.
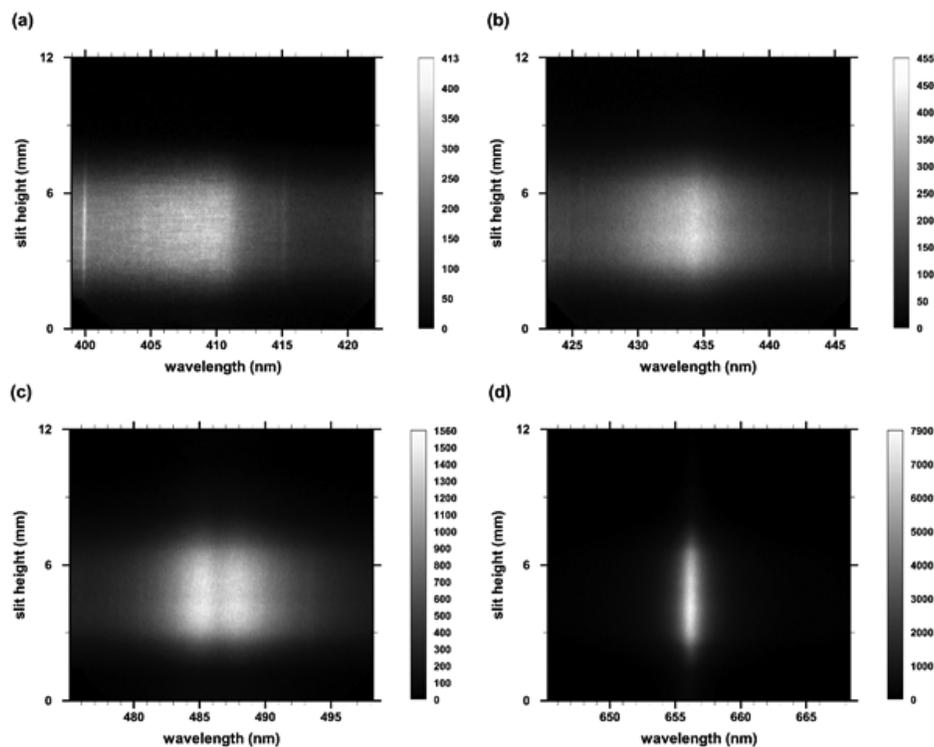
Figure 1: Recorded Balmer series hydrogen lines at 0.75-µs time delay, 0.025-µs gate. (a) Hδ, (b) Hγ, (c) Hß, and (d) Hα
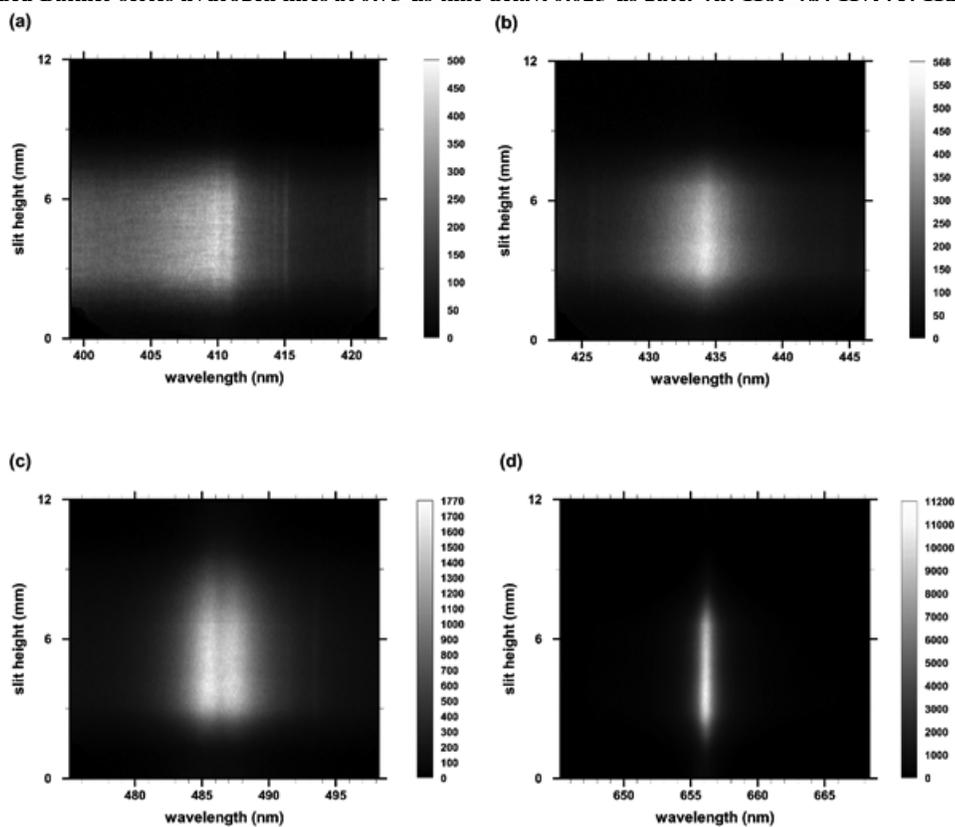
Figure 2: Recorded Balmer series hydrogen lines at 1.5-µs time delay, 0.025-µs gate. (a) Hδ, (b) Hγ, (c) Hβ, and (d) Hα
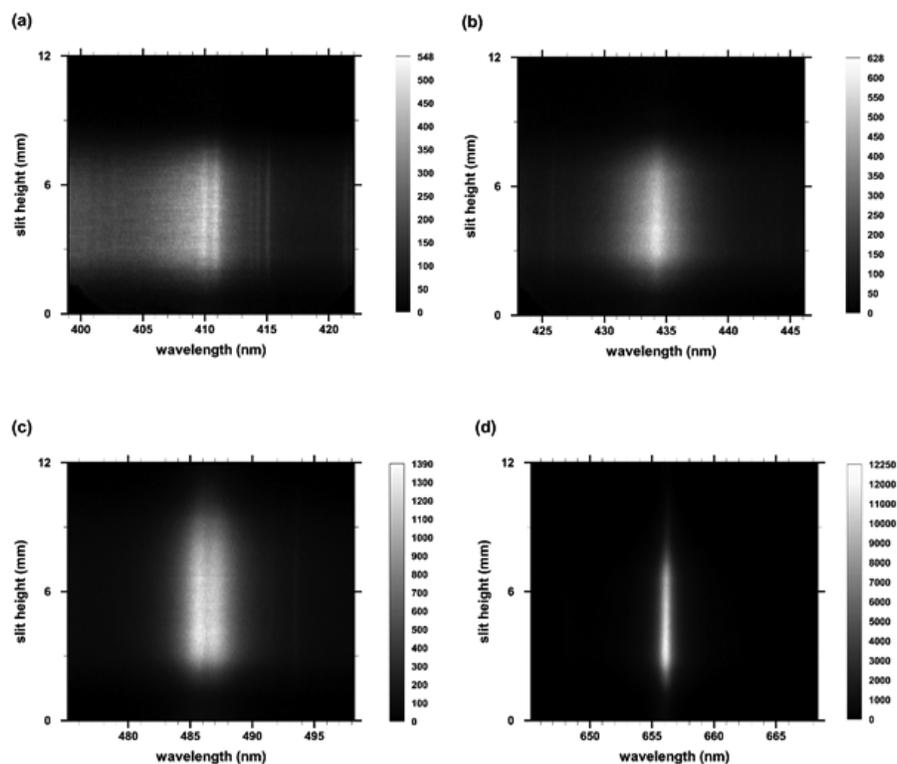
Figure 3: Recorded Balmer series hydrogen lines at 2.25-μs time delay, 0.025-μs gate. (a) Hδ, (b) Hγ, (c) Hβ, and (d) Hα
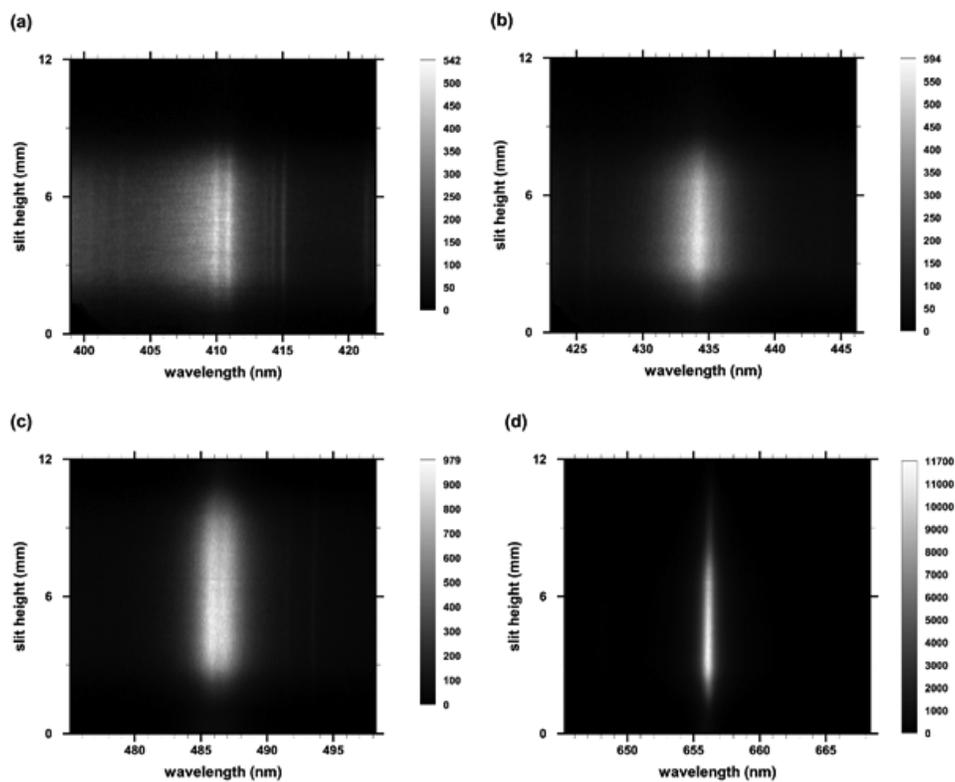
Figure 4: Recorded Balmer series hydrogen lines at 3-μs time delay, 0.025-μs gate. (a) Hδ, (b) Hγ, (c) Hβ, and (d) Hα

3.2 Hδ and Hγ line profiles

The analysis of the Hδ and Hγ data relies on computer simulations [15], and in this work, on published Stark tables [10] that show electron-density data in the range of 0.1 to 1×10^{17} cm^{-3} for a temperature of 20 kK. From the Stark tables, Hδ and Hγ line-profiles can be constructed for electron densities, N_e, of 0.1 and 1×10^{17} cm^{-3}. Figures 5 and 6 illustrate the line shapes of Hδ and Hγ, respectively. Subsequently, Hδ and Hγ FWHM can be determined for plasma diagnosis. Moreover, Hδ invites the use of peak separation (PS) as a diagnostic tool.

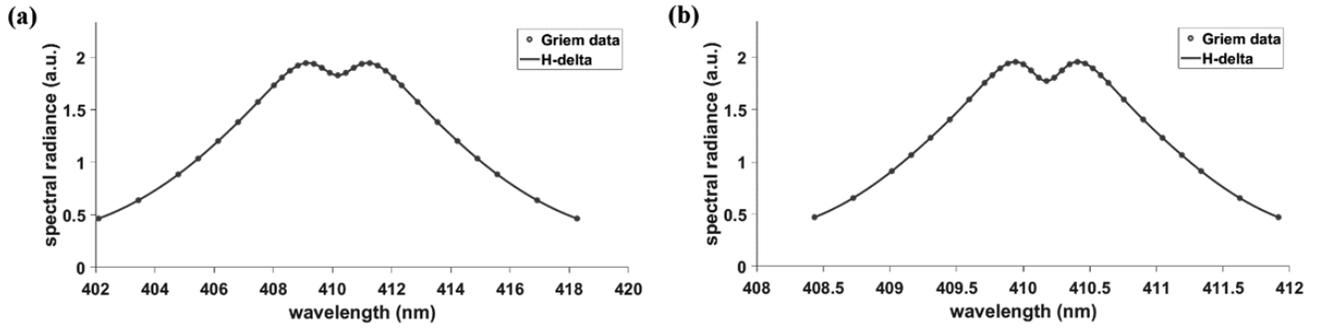**Figure 5: Line shapes of Balmer H at a temperature of 20 kK. (a) N = 1×10^{17} cm^{-3} , FWHM: 10 nm, PS: 2.0 nm. (b) N = 0.1 × 10^{17} cm^{-3} , FWHM: 2.2 nm, PS: 0.5 nm**
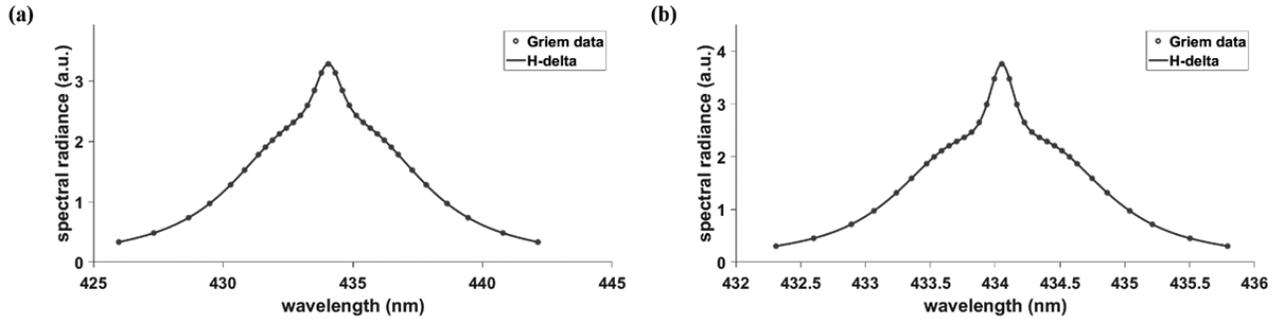

Figure 6: Line shapes of Balmer H at a temperature of 20 kK. (a) N = 1×10^{17} cm^{-3}, FWHM: 6.0 nm. (b) N = 0.1 × 10^{17} cm^{-3} , FWHM: 1.15 nm

From log-log fitting of Hδ and Hγ tables, see Figs. 5 and 6, in the range of 0.1 to 1×10^{17} cm^{-3} , one obtains for the Hδ FWHM, $\Delta\lambda_\delta$,

$$\Delta\lambda_\delta[\text{nm}] \ = 10 \left(\frac{N_e[\text{cm}^{-3}]}{10^{17}} \right)^{0.67} \tag{6}$$

The Hδ peak-separation, $\Delta\lambda_{\delta\text{-ps}}$, in the range of 0.1 to 1×10^{17} cm^{-3} amounts to

$$\Delta\lambda_{\delta-ps}[\text{nm}] \ = 2 \left(\frac{N_e[\text{cm}^{-3}]}{10^{17}} \right)^{0.62} \tag{7}$$

The Hδ shows peak separations just like those for the Hβ line [22]. The appearance of the Hγ line is perhaps

unusual in view of the Hα line, but Fig. 6 portrays the line-shape modifications due to the Stark effect. From log-log fitting, one obtains for FWHM of Hγ, $\Delta\lambda_\gamma$,

$$\Delta\lambda_\gamma [nm] = 6 \left(\frac{N_e [cm^{-3}]}{10^{17}} \right)^{0.72} \tag{8}$$

3.3 Abel-inverted spectral maps

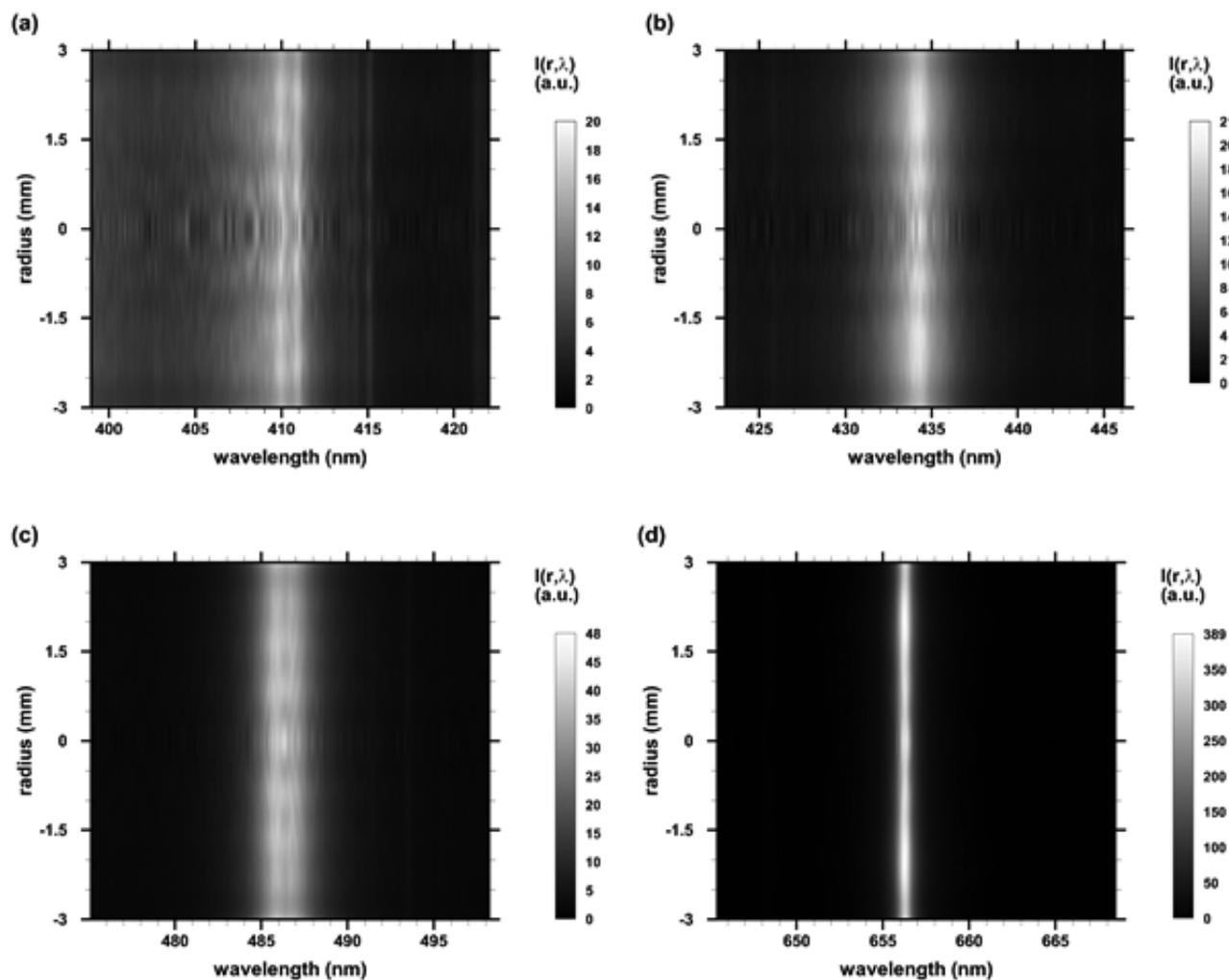**Figure 7: Abel-inverted Balmer series hydrogen lines at 3-μs time delay, 0.025-μs gate. (a) Hδ, (b) Hγ, (c) Hβ, and (d) Hα**

The recorded line-of-sight data are further processed using inverse Abel transform in order to examine the spatial distribution of the expanding plasma. The wavelength variation along the slit dimension is corrected for each spectral line of a single slit-height versus wavelength map. Consequently, the maps (see Figures 1 to 4) are primed for analysis of integral inversion of the recorded line-of-sight data. Figures 7 and 8 illustrate the spectral radiance as function of radius and wavelength for time delays of 3 and 1.5 μs, respectively.
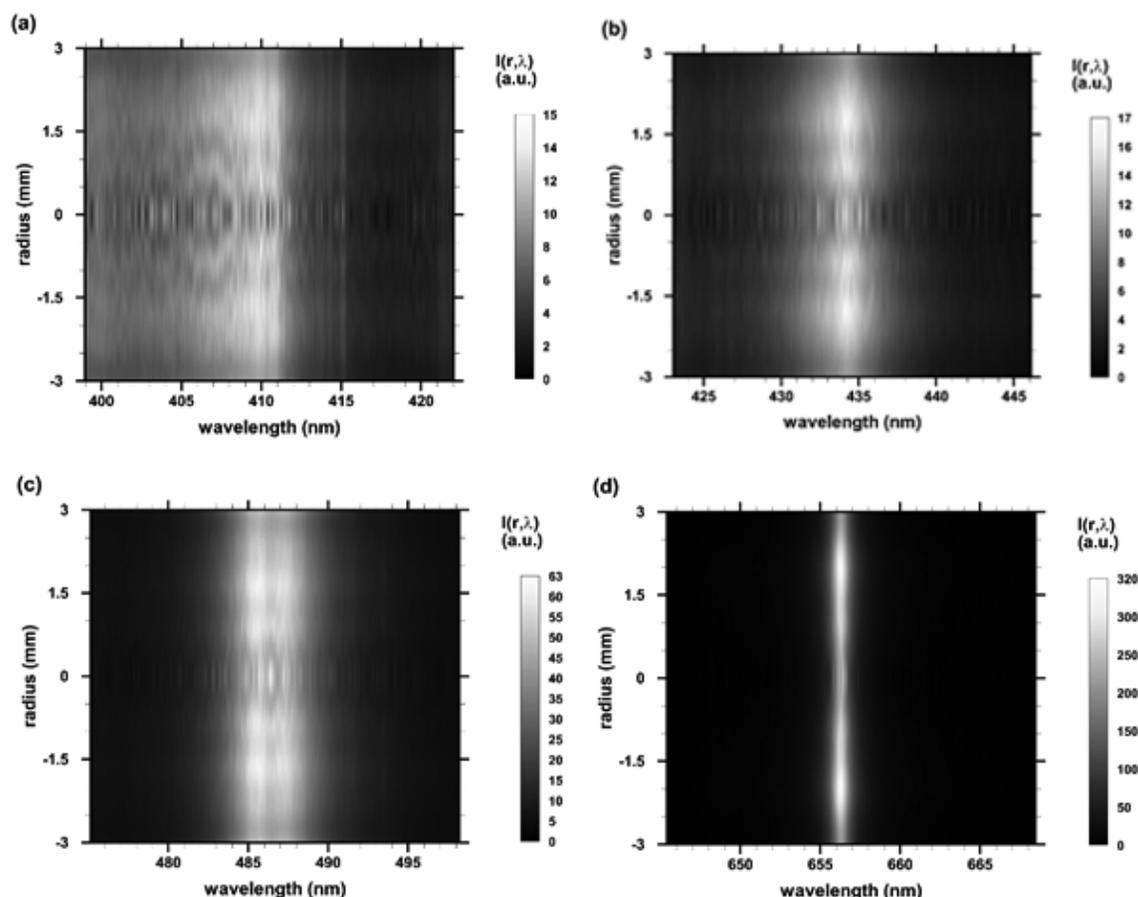
Figure 8: Abel-inverted Balmer series hydrogen lines at 1.5-μs time delay, 0.025-μs gate. (a) Hδ, (b) Hγ, (c) Hβ, and (d) Hα

The measured line-of-sight, central spectral regions of appear almost symmetrical with-respect-to the slit height. Abel-inversions utilize the analysis method previously communicated for ultra-pure hydrogen experiments [23]. The Abel-inverted, 3-μs time-delay data display reasonably smooth lineshapes for all four Balmer series lines. The Hδ peak separation can be easily demarcated, but the Hβ peak separation is difficult to extract. In other words, The Hδ line provides both peak separation and FWHM diagnostics as the electron density decreases in the range of 1 to 0.1×10^{17} cm^{-3}. From Equation (7), a 1-nm peak separation of the Hδ line in Fig. 7 implies $N_e = 0.33 \times 10^{17}$ cm^{-3}.

For the 1.5 μs data, the Abel-inverted, first four Balmer series lines reveal minima at the center of the plasma. These minima are representative of plasma expansion phenomena following initiation of optical breakdown. Figures 8a and 8c reveal peak separations of the Hδ and Hβ lines, respectively. The Hδ map also indicates that the background is shaded towards the uv, and there appear to be contributions from the Hε line (at the low wavelength side in the map). The Hδ line shows a shallower dip for higher electron density as illustrated in Figure 5 in the range of 0.1 to 1×10^{17} cm^{-3}. However, the Hβ peak separation indicates an electron density of 1.5×10^{17} cm^{-3}.

Both Figures 7 and 8 indicate undulations of the signal along the radial direction. Such undulations can be expected as the laser-plasma expands – in related experiments of optical breakdown in air, multiple reflections can be seen in shadowgraphs that are captured following optical breakdown in air. Similar behavior is expected to occur for the hydrogen:nitrogen mixture. Figure 9 displays recorded air-breakdown shadowgraph to further elucidate multiple reflections that are likely causing undulations in the plasma core. The shadowgraph experiments recorded 125 images for each time delay, using a factor of five larger irradiances than those for the hydrogen:nitrogen expoeriments. The selected images portray typical images.
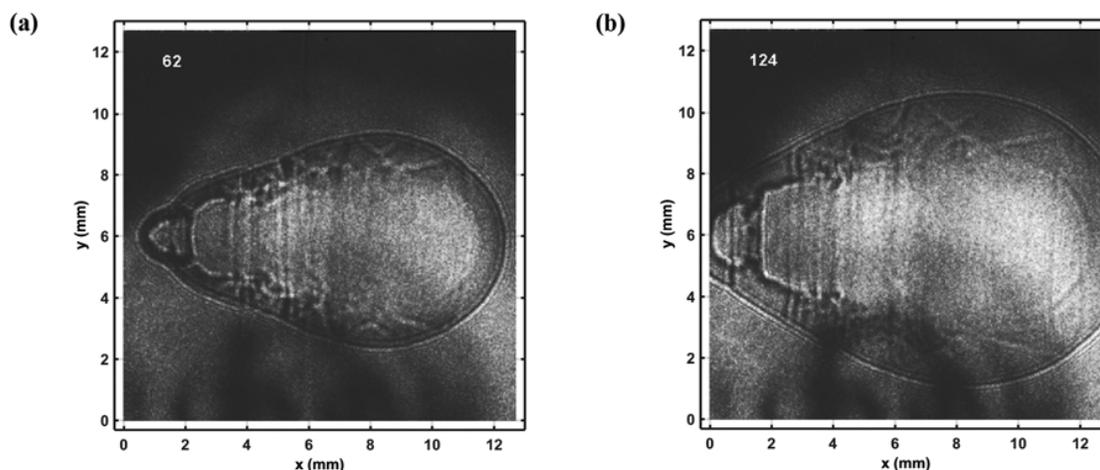
Figure 9: Shadowgraph of optical breakdown in laboratory air. The laser beam propagates from the right, images are captured using a second, imaging laser. The "bubble" on the laser side indicates absorption of laser radiation. Time delay: (a) 1.5 μs, image 62. (b) 3 μs, image 124

3.4 Electron temperature and density

Analysis of the recorded spectra along the slit height aims to evaluate electron temperature, T, from Boltzmann plots. Moreover, electron density, N_e, determination relies on formulae and tables that describe Stark broadening in laser-plasma.

Figure 10 portrays typical Boltzmann plots from line-of-sight measurements at time delays of 2.25 and 3.25 μs. The method utilizes Boltzmann distributions and determination of the slope to extract the temperature from the negative of 1/slope. The intercept of the straight line is not used for evaluation of the temperature. For data points from the four Balmer series members close to the fitted line, one can infer local thermodynamic equilibrium. As the data points deviate from the fitted line, deviations from equilibrium may be concluded – self-absorbed lines would also cause deviations of data points from the straight line, and equally, ambiguities in determination of the baseline. However, expansion dynamics may lead to variations in the integrated line intensities leading to a 25% estimate for the accuracy of the inferred temperature.
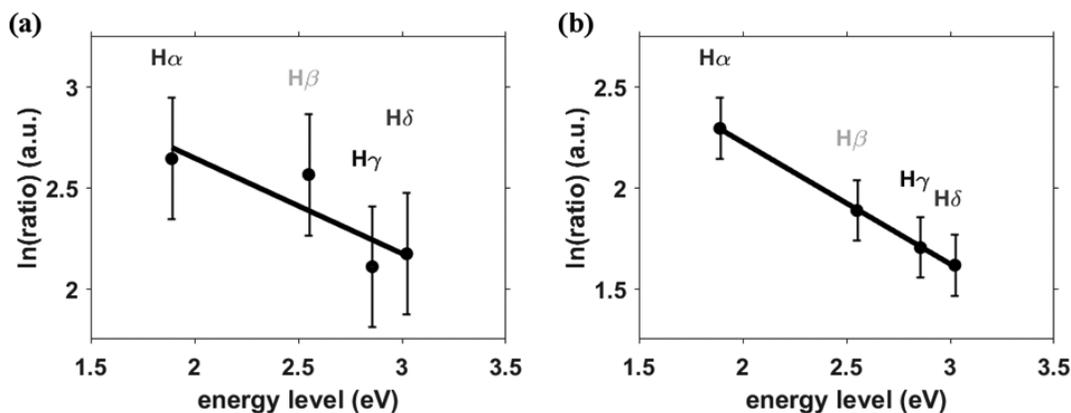

Figure 10: Boltzmann plot from line-of-sight data at 4.8-mm slit height. (a) T = 26.5 kK, time delay 1.5 μs (see Fig. 2). (b) T = 19.3 kK, time delay 3.25 μs (see Fig. 4)

The electron density is related to the hydrogen Balmer series FWHM to the power of the order of 1.5, however, detailed theory predictions and experimental results indicate slight deviations. Empirical equations are obtained from log-log fitting of FWHM and electron density. For red-shift of the Hα line, the dependency on electron density is almost linear. Significant new results also utilize peak-separation of the Hβ line to find N_e. Stark broadening widths increase from Hα to Hδ. The use of Hδ peak-separation for N_e determination in laser-plasma adds a new diagnostic tool. Investigations of the Hδ peak separation is communicated for N_e in the range of 0.1 to 1×10^{17} cm^{-3} and for the hydrogen-nitrogen laser plasma. Table 1 displays measured FWHM and peak-separations. Table 2 reports the corresponding electron densities.

Table 1: Balmer series FWHM and Hδ and Hβ peak-separations – line-of-sight data at 4.8-mm slit height.

τ [μs]	$Ä_δ$	$Δλ_{δ\text{-ps}}$ [nm]	$Δλ_γ$ [nm]	$Δλ_β$ [nm]	$Δλ_{β\text{-ps}}$ [nm]	$Δλ_α$ [nm]
1.5	7.5 ± 1.5	1.4 ± 0.8	5.0 ± 0.2	4.3 ± 0.25	1.2 ± 0.2	1.17 ± 0.1
3.25	5.8 ± 0.3	1.1 ± 0.2	3.2 ± 0.2	2.6 ± 0.25	0.8 ± 0.15	0.78 ± 0.1

Table 2: First four Balmer series electron densities, N_e [10^{17} cm^{-3}], from line-of-sight data at 4.8-mm slit height.

τ [μs]	N_e (δ)	N_e (δ-ps)	N_e (γ)	N_e (β)	N_e (β)	N_e (α)	Average N_e
1.5	0.65	0.56	0.77	0.91	0.88	0.84	0.77
3.25	0.44	0.38	0.41	0.46	0.46	0.45	0.43

The values are determined from the spectra at a slit height of 4.8 mm by using Matlab software 'peakfit.m' [24]. An analogous fitting approach accomplishes determination of the areas of the four lines, but corrections are applied for the area due to the recording of only the central portion of the lines. While the wings of hydrogen lines may not be Lorentzian, the analysis in this work relies on Lorentzian line shapes for estimates of the area corrections that are give-or-take 10 per cent.
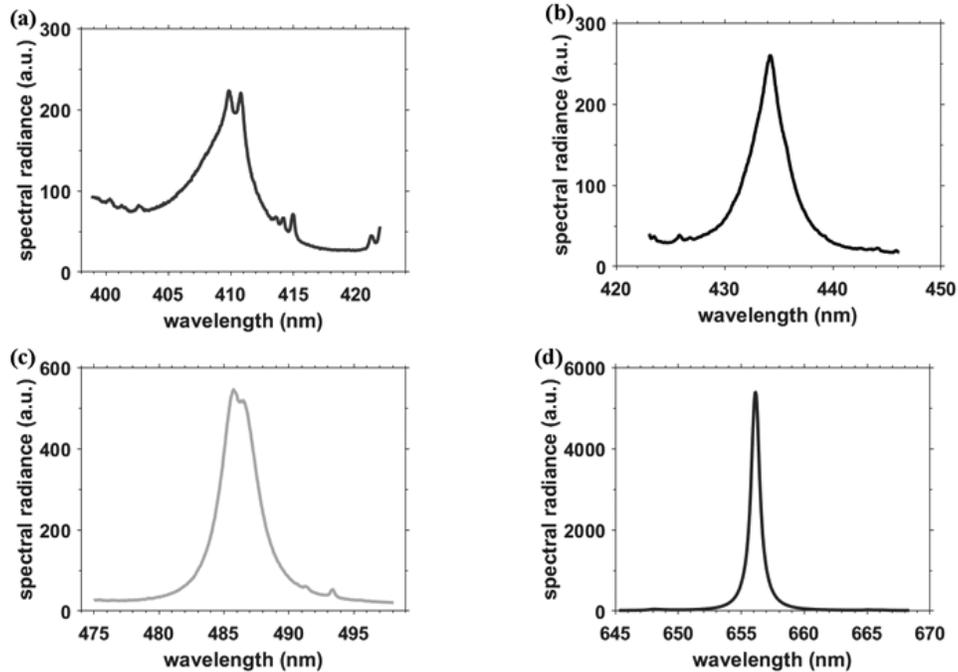
Figure 11: Average line shapes for τ = 3 μs. (a) Hδ, (b) Hγ, (c) Hβ, and (d) Hα

Line shapes that are averaged along the slit dimension display spectra that would be obtained without spatial resolution of the plasma along the axial direction, viz. slit dimentsion. Figure 11 illustrates the line-shapes averaged alonge the slit dimension.

For the 3.25-µs time delay, electron densities largely agree when inferred from the widths of the four Balmer series lines and from the peak-separations of Hδ and Hβ. However, there are subtle differences of N_e determined at 1.5-µs time delay. One may conclude from the appearance of the measured emission spectra and the computed Abel-inverted spectra that super- to hyper- sonic laser-plasma expansion speeds affect the establishment of local thermodynamic equilibrium. Details are investigated in the next section.

3.5 Plasma expansion dynamics

Laser-plasma generation with laser pulses of the order of 10 ns and pulse energies of 80 in 800 mJ ambient laboratory conditions causes a shock wave that expands at a rate of one to a few mm per µs, or a few km/s, for time delays of the order of 1 µs. Early in the plasma decay, expansion speeds of up to 80 km/s are usually encountered that may be described in engineering terms as well above re-entry speeds or high hypersonic speeds. Several tens of microseconds after plasma initiation, the shock wave reduces to the speed of sound.

In view of the "bubble" expanding in air and the associated isentropic expansion, one can determine electron density or temperature to elucidate the phenomena. Captured shadowgraphs can guide time-resolved spectroscopy, however, there should be an indication of the shockwave in spatially- and temporally- resolved measured spectra. One approach may utilize Radon- or Abel- inversion techniques [8] that are generally known as computed tomography methods. Or one may closely investigate the captured spectra along the slit height.

Systematic determination of the Stark widths from line-of-sight data is expected to reveal an higher electron density near the shock wave than in the plasma core. Alternatively, determination of the area of the atomic Balmer series lines should indicate higher temperature near the shock wave than in the plasma center. Moreover, for time delays of several µs – as the shockwave expanded beyond the interrogated volume – the plasma is expected to be "homogeneous and indicate local thermodynamic equilibrium for electron densities excess of 0.1 ×", as indicated by the necessary McWhirter criterion [3, 4], but with higher temperature in the core.

Figures 12 compares electron density results for a time delay of 1.5µs. Increases in electron density at the plasma edges are indications of the expanding shock wave. In order to estimate the shock wave radius as function of time delay, τ, it is advantageous to utilize the Taylor-Sedov formula [25] for spherically expanding plasma,

$$R(\tau) = \left(E_p \,/\rho \;\; \tau^2\right)^{1/5} \tag{9}$$

where the laser-pulse energy, E_p, for the experiments amounts to 0.15 J, and the density of the 1:1 nitrogen-hydrogen mixture, ρ, equals 0.37 kg/m³. For τ = 1.5 µs, one finds for the radius R = 4 mm.
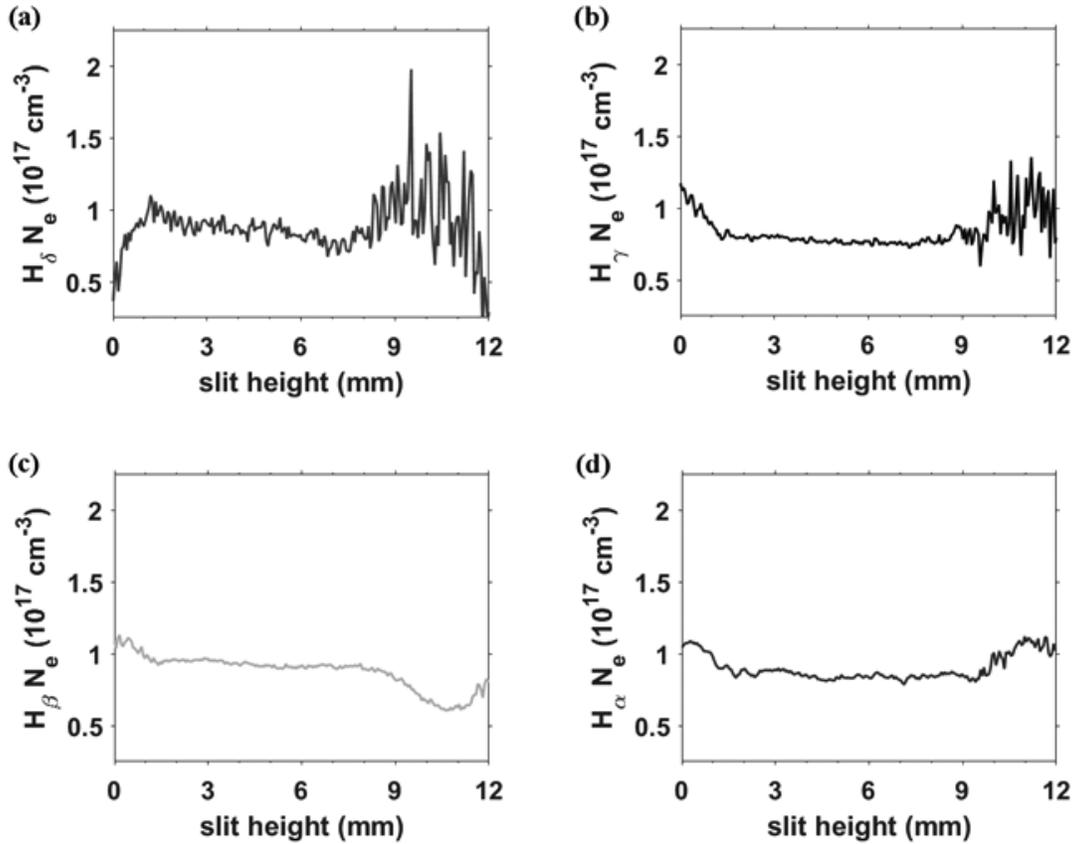
Figure 12: Electron density from line-of-sight data displayed in Figure 2 at = 1.5 μs, 0.025-μs gate. (a) Hα, (b) Hβ, (c) Hγ, and (d) Hδ

The electron density variation along the slit dimension indicates that the electron density determined from Hβ is smaller than that obtained from Hα for slit heights larger then 9 mm. This result may be associated with variations induced along the shock wave front. Further investigation is aimed at determining the electron temperature variation. Figure 13 illustrates spectroscopic snapshots of the determined temperature for 1.5μs and 2.5μs time delays. The snapshots, computed from Boltzmann plots and for equally-weighted contributions from all four lines, illustrate that noticeable expansion occurs towards the incoming laser beam and propagates towards the top of the slit height near 12 mm in Figure 13.
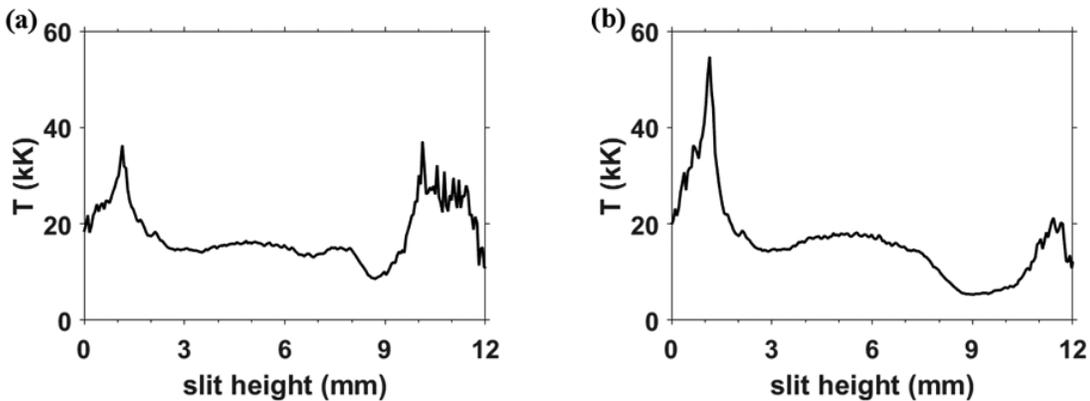

Figure 13: Electron temperature from line-of-sight data. (a) τ = 1.5 μs, 0.025-μs gate. Average temperature: 17.9 kK. (b) τ = 2.5 μs, 0.025-μs gate. Average temperature: 16.3 kK

4. DISCUSSION

The experimental study of Hδ and Hγ line shapes shows that results are obtained that are consistent with those from Hβ and Hα, especially for time delays of the order of a few μs after initiation of laser-plasma. Shock waves tend to propagate at speeds of the order of one mm/s for the 0.27-atm hydrogen nitrogen mixture. Investigations of time-resolved spectra for time-delays of the order of 0.25 to 1.5 μs reveal effects from the expanding shock wave. Analysis of spectra that are recorded along the slit dimension indicate a temperature profile that is expected from computations of shock wave expansions. Abel-inverted spectra confirm the shock-wave related increase of temperature and electron density, including a reduced temperature and density profile in the center of the expanding micro-plasma.

The explored Hδ and Hγ lines can provide additional diagnostics laser-plasma and for analysis of white dwarf spectra, especially in the range of 0.1 to 1×10^{17} cm^{-3}. However, when using all four lines of the Balmer series, bound-free opacity corrections would be required for comparisons of laboratory emission with white dwarf absorption spectra. In conclusion, analysis of white-dwarfs and other astrophysical objects such as active galactic nuclei from only one line, i.e., Hα, may be preferred as bound-free effects may not be significant across one line for purposes of determinations of the Hα width and asymmetry. Future work however should include new results from laboratory measurements that address specifically the shapes of lines for diagnosis of astrophysics phenomena.

References

[1] A.W. Miziolek, V. Palleschi, I. Schechter, Eds. *Laser Induced Breakdown Spectroscopy*, Cambridge University Press: New York, NY, USA, 2006.

[2] J.P. Singh, S.N. Thakur, Eds. *Laser Induced Breakdown Spectroscopy*, Elsevier Science: New York, NY, USA, 2019; in press.

[3] R.W.P. McWhirter. Spectral Intensities. In *Plasma Diagnostic Techniques*, Huddlestone, R.H., Leonard, S.L., Eds., Academic Press: New York, NY, USA, 1965; pp. 201 – 264.

[4] G. Cristoforetti, A. De Giacomo, M. Dell'Aglio, A. Legnaioli, E. Tognoni, V. Palleschi, N. Omenetto. *Spectrochim. Acta Part B: At. Spectrosc.* 65, 86 (2010).

[5] W.L. Wiese. Line Broadening. In *Plasma Diagnostic Techniques*, Huddlestone, R.H., Leonard, S.L., Eds.; Academic Press, New York, NY, USA, 1965; pp. 265–317.

[6] T. Fujimoto. *Plasma Spectroscopy*, Clarendon Press: Oxford, UK, 2004.

[7] H.-J. Kunze. *Introduction to Plasma Spectroscopy*, Springer: New York, NY, USA, 2009;

[8] G. Pretzler, H. Jäger, T. Neger, H. Philipp, J. Woisetschläger. *Z. Naturforsch.* 47a, 955 (1992).

[9] P.-E.Tremblay, P. Bergeron. *Astrophys. J.* 696, 1755 (2009).

[10] H.R. Griem. *Spectral Line Boradening by Plasmas*, Academic Press: Cambridge, MA, USA, 1974.

[11] J. Halenka, W. Olchawa, J. Madej, B. Grabowski. *Astrophys. J.* 808, 131 (2015).

[12] C.G. Parigger, K.A. Drake, C.M. Helstern, G. Gautam. *Atoms* 6, 6030036 (2018).

[13] C.G.Parigger, C.M. Helstern, G. Gautam. *Int. Rev. At. Mol. Phys.* 8(1), 25 (2017).

[14] C.G. Parigger, A.C. Woods, M.J. Witte, L.D. Swafford, D.M. Surmick. *J. Vis. Exp.* 84, e51250 (2014).

[15] M.A. Gigosos, M. Á. González, V. Cardeñoso. *Spectrochim. Acta B At. Spectrosc.* 58, 1489 (2003).

[16] J. Holtsmark, *J. Ann. Phys.* 58, 577 (1919).

[17] R.E. Greene, R.E. Jr. *The Shift and Shape of Spectral Lines*, Pergamon Press: Oxford, UK, 1961, Chap. 4, pp.118–193.

[18] E. Oks. *Diagnostics of Laboratory and Astrophysical Plasmas Using Spectral Lineshapes of One-, Two-, and Three-Electron Systems*, World Scientific: Singapore, 2017, pp. 1-47.

[19] E. Schrödinger. *Ann. Phys.* 385, 437 (1926).

[20] The Nobel Prize in Physics 1933. Available online: https://www.nobelprize.org/prizes/physics/1933/summary/ (accessed on May 24 2019).

[21] D.R. Inglis, E. Teller. *Astrophys. J.* 90, 439 (1939).

[22] M. Ivkovic, N. Konjevic, Z.J. Pavlovic. *J. Quant. Spectrosc. Radiat. Trans.* 154, 1 (2015).

[23] C.G. Parigger, G. Gautam, D.M. Surmick. *Int. Rev. At. Mol. Phys.* 6(1), 43 (2015).

[24] T.C. O'Haver. Command-line peak fitter for time-series signals. Version 9.0, January 2018; Mathworks File Exchange; Available online: https://www.mathworks.com/matlabcentral/fileexchange/23611-peakfit-m (accessed June 4 2019).

[25] G.I. Taylor. *Proc. Roy. Soc. A* 201, 175 (1950).